Upwind–Downwind Asymmetry of the Sea Backscattering Normalized Radar Cross Section Versus the Skewness Function

Christophe Bourlier

***Abstract*— From the first-order small slope approximation, this paper presents a closed-form expression of the sea backscattering normalized radar cross section (NRCS) versus the skewness function to predict the upwind–downwind asymmetry. This effect is produced by the fact that the surface height distribution slightly deviates from a Gaussian one. Introducing the azimuthal property of the sea height autocorrelation and skewness (spatial) functions, the integration over the azimuthal direction can be done analytically, whereas the integration over the radial distance can be done using the property that the skewness correlation distance is much smaller than that of the gravity waves. Then, the backscattering NRCS is expressed from the sea skewness spectrum at a wavenumber different of the Bragg wavenumber. In addition, a simple inversion algorithm is proposed to perform the parameters of the skewness function from experimental data in C and K_u bands.**

***Index Terms*— Radar scattering remove, remote sensing, sea surface electromagnetic scattering.**

I. Introduction

TODAY, satellite remote sensing opens the possibility of characterizing the ocean surface both at global scale and at fine resolution, using active or passive instruments. Following the recent improvements in techniques and theories, links have been established between the normalized Radar cross section (NRCS) of the sea surface associated with the respective backscattered or emitted microwave signals and a large number of oceanic parameters, such as wind speed and direction, wave heights and slopes, wave spectrum, surface current, temperature, and salinity. However, the success of the inversion procedure relies crucially on an accurate phase resolving statistical description of the sea surface topography. In this respect, non-Gaussian characteristics of short wind waves are of primary importance, as they have a strong influence on the microwave radar return. For instance, to predict the asymmetry of the backscattering NRCS between the upwind and downwind directions, the assumption of a sea Gaussian height distribution is no longer valid and the higher order statistics must be accounted for. The departure from Gaussian statistics can be limited to the skewness and kurtosis of wave heights and slopes, involving the third (related to the skewness effect) and fourth (related to the peakedness effect) moments of the distributions. This is consistent with the well-known Cox and Munk slope distribution [1].

On the other hand, any simulation or interpretation of backscattering NRCS is bound to a scattering model, which should be able to cover a large variety of sea state conditions and account for the relevant geophysical parameters. In the last decade, many progresses have been made in scattering models from the sea surface with the construction of so-called unified models, such as first-order small slope approximation (SSA1) [2]–[4], SSA (first- and second-order SSA) [5]–[11], weighted curvature approximation [4], [12]–[15], and resonant curvature approximation [16], [17]. These models can operate a dynamical transition between the different asymptotic regimes like geometrical optics, derived from the Kirchhoff approximation and valid near the nadir, and small perturbation method (SPM)—valid for backscattering angles larger than approximatively 45°—without the introduction of a scale dividing wavenumber, which occurs in the well-known two-scale model [18], [19].

The statistical properties (sea height spectrum, height and slope distributions, and so on) of the sea surface can be determined from direct measurements of surface elevations [20], [21] or from optical [1], [22] or/and microwave measurements [23]–[25] if the inversion procedure is not too complex, which requires simple forward backscattering models.

For $f = 14.6$ GHz and $u_{10} = \{5, 15\}$ (wind speed at 10 meters above the sea mean level), Voronovich and Zavorotny [6] have compared the SSA1 with the full SSA (the second-order SSA is accounted for via the phase perturbation technique). For incidence angles $\theta \in [0; 60]°$, they observed that the SSA1 and SSA NRCSs are close for the vertical-vertical (VV) polarization, whereas for the horizontal-horizontal (HH) polarization, the difference between the SSA and SSA1 is positive and increases with the wind speed, but remains within about 2 dB. For $f = \{5.3, 14\}$ GHz and $u_{10} = \{5, 10\}$, McDaniel [7, Figs. 4 and 5] and Bourlier and Pinel [9, Fig. 1] predict a maximum deviation between the partial SSA (only the ladder term is accounted for, i.e., the correlation between the first- and second-order backscattered fields) and SSA1 of the order of 0.6 and 1.1 dB for the VV and HH polarizations, respectively. Therefore, the SSA1 model can predict the backscattering NRCS with a precision of 1 and 2 dB for

Manuscript received April 3, 2017; revised May 11, 2017; accepted June 5, 2017. Date of publication October 26, 2017; date of current version December 27, 2017.

The author is with the Institut d'Electronique et de Télécommunications de Rennes Laboratory, LUNAM UBL Université, Université de Nantes, Polytech Nantes, 44306 Nantes, France (e-mail: christophe.bourlier@univ-nantes.fr).

Color versions of one or more of the figures in this paper are available online at http://ieeexplore.ieee.org.

Digital Object Identifier 10.1109/TGRS.2017.2713990

the VV and HH polarizations, respectively. As shown in [17], for the calculation of the copolarizations ratio, the surface curvature effect must be included in the scattering model to better predict the backscattering NRCS for the HH polarization.

From microwave measurements [26]–[29] and for the copolarizations (VV and HH), the backscattering NRCS is modeled as $\sigma(u,\theta,\phi) = \sigma_0(u,\theta) + \sigma_1(u,\theta)\cos(\phi) + \sigma_2(u,\theta)\cos(2\phi)$, where θ is the radar incidence angle, ϕ is the wind direction relative to the radar azimuth look direction, and u is the near-surface wind speed. By introducing the skewness and peakedness spatial functions, Bourlier [3] showed that this decomposition is consistent with the SSA1 scattering model and that the first-order coefficient σ_1 is related to the skewness function. If the skewness effect is neglected, then $\sigma_1 = 0$. In this paper, using the property that the skewness correlation distance is much smaller than that of the gravity waves, a forward simple model of σ_1 is derived versus the skewness function, and then, a simple inversion algorithm is proposed to perform the parameters of the skewness function from experimental data in C [27], [28] and K_u [26], [29] bands.

This paper is organized as follows. Section II presents the SSA1 backscattering NRCS. Section III defines the skewness spatial function and its spectrum. Section III derives a closed-form expression of the backscattering NRCS. Section V presents numerical comparisons with experimental data.

II. SSA1 Backscattering NRCS

From SSA1, for a non-Gaussian height distribution and for the copolarizations (VV and HH), Bourlier [3] showed that the coefficients $\{\sigma_0, \sigma_1, \sigma_2\}$ are expressed as

$$\begin{cases} \sigma_0 = \dfrac{2|\mathcal{B}_1|^2 e^{-Q_z^2\sigma_z^2}}{Q_z^2}\displaystyle\int_0^\infty [e^{\alpha_0}\Omega_0(\alpha_1,\alpha_2) - 1]J_0(Q_H r) r dr \\ \sigma_{1,2} = \dfrac{4|\mathcal{B}_1|^2 e^{-Q_z^2\sigma_z^2}}{Q_z^2}\displaystyle\int_0^\infty e^{\alpha_0}\Omega_{1,2}(\alpha_1,\alpha_2)J_{1,2}(Q_H r) r dr \end{cases} \tag{1}$$

where

$$\begin{cases} \Omega_0(\alpha_1,\alpha_2) = J_0(\alpha_1)I_0(\alpha_2) \\ \Omega_1(\alpha_1,\alpha_2) = -J_1(\alpha_1)I_0(\alpha_2) + I_1(\alpha_2)\left[J_1(\alpha_1) - J_3(\alpha_1)\right] \\ \Omega_2(\alpha_1,\alpha_2) = +J_2(\alpha_1)I_0(\alpha_2) + I_1(\alpha_2)\left[J_0(\alpha_1) + J_4(\alpha_1)\right] \end{cases} \tag{2}$$

and

$$\begin{cases} \alpha_0(r) = Q_z^2 C_{z0}(r) + \dfrac{Q_z^4 C_{p0}(r)}{2} \\ \alpha_1(r) = Q_z^3 C_{s0}(r) \\ \alpha_2(r) = Q_z^2 C_{z2}(r). \end{cases} \tag{3}$$

Moreover, $Q_z = 2K\sin\theta$, $\mathcal{B}_1$ is the polarization term of the first-order SPM, J_n is the Bessel function of first kind and nth order, whereas I_n is the Bessel function of second kind and nth order.

The functions $C_s(r,\psi) = C_{s0}(r)\cos\psi$ and $C_p(r,\psi) = C_{p0}(r)$ are the spatial skewness and peakedness functions, respectively, defined as

$$\begin{cases} C_s(r,\phi) = C_{s0}(r)\cos\phi = \dfrac{1}{6}\left\langle z_1 z_2^2 - z_1^2 z_2\right\rangle \\ C_p(r,\phi) = C_{p0}(r) = \dfrac{1}{12}\langle (z_1 - z_2)^4\rangle - \left[\sigma_z^2 - C_z(r,\phi)\right]^2. \end{cases} \tag{4}$$

The functions C_{s0} and C_{p0} stand for the isotropic part of C_s and C_p, respectively. Moreover, to be consistent with the measurements of the slope distributions in [1] (see the next section), the peakedness function is assumed to be isotropic, whereas the skewness function depends on $\cos\phi$, where ϕ is the azimuthal direction along the wind direction. The surface elevation $z_i = z(\boldsymbol{r}_i) = z(x_i, y_i)$ and the ensemble average operator $\langle\cdots\rangle$ depend only on $\boldsymbol{r} = \boldsymbol{r}_2 - \boldsymbol{r}_1 = (x, y)$ as the sea surface is assumed to be homogeneous.

In polar coordinates, $(x, y) = (r\cos\phi, r\sin\phi)$, the isotropic C_{z0} and anisotropic C_{z2} parts of the surface height autocorrelation function $C_z(r,\phi) = \langle z_1 z_2\rangle = C_{z0}(r) - \cos(2\phi)C_{z2}(r)$ (second-order statistical moment) are expressed from the isotropic $\hat{C}_{z0}$ and anisotropic $\hat{C}_{z2} = \hat{C}_{z0}\hat{\Delta}(k)$ parts of the surface height spectrum $[(k_x, k_x) = (k\cos\psi, k\sin\psi)]$ as

$$\begin{cases} C_{z0}(r) = \displaystyle\int_0^\infty \hat{C}_{z0}(k)J_0(kr)dk \\ C_{z2}(r) = \displaystyle\int_0^\infty \hat{C}_{z0}(k)\hat{\Delta}(k)J_2(kr)dk. \end{cases} \tag{5}$$

If $\alpha_1 = 0$, then from (2), $\Omega_1(\alpha_1,\alpha_2) = 0$, which leads to $\sigma_1 = 0$. This shows that the skewness effect is responsible of the asymmetry between the up- ($\phi = 0$) and downwind ($\phi = 180°$) directions. Equations (1) and (3) also show that the peakedness effect is linked to C_{z0}. From SSA1, this means that the isotropic part of the sea height spectrum cannot be retrieved, but only from the sum $C_{z0}(r) + Q_z^2 C_{p0}(r)/2$.

From numerical simulations, Bourlier [3] showed that the skewness effect is minor on the NRCS coefficients $\{\sigma_{0,2}\}$, which leads from (2) to

$$\begin{cases} \Omega_0(\alpha_1,\alpha_2) \approx \Omega_0(0,\alpha_2) = I_0(\alpha_2) \\ \Omega_1(\alpha_1,\alpha_2) = -J_1(\alpha_1)I_0(\alpha_2) + I_1(\alpha_2)\left[J_1(\alpha_1) - J_3(\alpha_1)\right] \\ \Omega_2(\alpha_1,\alpha_2) \approx \Omega_2(0,\alpha_2) = I_1(\alpha_2). \end{cases} \tag{6}$$

In what follows, the peakedness effect is neglected, which means that $\alpha_0(r) \approx Q_z^2 C_{z0}(r)$.

III. Skewness Function

A. Skewness Spectrum

As the surface height (spatial) autocorrelation function, the surface skewness spatial function $C_s(\boldsymbol{r})$ can be expressed in the Fourier domain, giving the surface skewness spectrum $\hat{C}_s(\boldsymbol{k})$. It is defined as

$$\begin{aligned} \hat{C}_s(\boldsymbol{k}) &= \int C_s(\boldsymbol{r})e^{-j\boldsymbol{k}\cdot\boldsymbol{r}}d\boldsymbol{r} \\ &= \int_0^\infty\int_0^{2\pi} rC_s(r,\phi)e^{-jkr\cos(\psi-\phi)}drd\phi \\ &= \int_0^\infty\int_0^{2\pi} \cos(\phi)rC_{s0}(r)e^{-jkr\cos(\psi-\phi)}drd\phi \end{aligned} \tag{7}$$

where $C_s(r,\phi) = \cos(\phi)C_{s0}(r)$. From (A3), the integration over ϕ gives

$$\hat{C}_s(\boldsymbol{k}) = -2\pi j\cos(\psi)\int_0^\infty rC_{s0}(r)J_1(kr)dr \tag{8}$$

where $J_1(-a) = -J_1(a)$.

In polar coordinates, to be consistent with the definition of the sea surface height spectrum, we have $\hat{C}_s(\boldsymbol{k})d\boldsymbol{k} = (2\pi)^2 k\hat{C}_s(k_x,k_y)dkd\psi = (2\pi)^2\hat{C}_s(k,\psi)dkd\psi$, leading to $\hat{C}_s(\boldsymbol{k}) = \hat{C}_s(k_x,k_y)/k$ and

$$\hat{C}_s(k,\psi) = -\frac{j\cos(\psi)}{2\pi}\hat{C}_{s0}(k) \tag{9}$$

where

$$\hat{C}_{s0}(k) = k\int_0^\infty rC_{s0}(r)J_1(kr)dr = -k\frac{\partial}{\partial k}\int_0^\infty C_{s0}(r)J_0(kr)dr \tag{10}$$

because $\partial J_0(kr)/\partial k = -rJ_1(kr)$. Since $\int_0^\infty kJ_1(kr)dk = 1/r^2$, the above also shows that

$$\int_0^\infty \hat{C}_{s0}(k)dk = \int_0^\infty \frac{C_{s0}(r)}{r}dr = P_{s0}. \tag{11}$$

The number P_{s0} (in cube meter) can be interpreted as the total power of the skewness surface heights. Equation (9) shows that the isotopic part of the skewness spectrum is imaginary since $\hat{C}_{s0}(k)$ is a real function.

We can show from (10) that the skewness spatial function is expressed from its spectrum as

$$C_{s0}(r) = \int_0^\infty \hat{C}_{s0}(k)J_1(kr)dk. \tag{12}$$

B. Spatial Skewness Function Near the Origin

Near the origin ($\boldsymbol{r}$ close to zeros), the spatial function C_{s0} can be expressed from the statistics moments of the Cox and Munk slope distribution by calculating the characteristic function of the surface slopes (γ_x,γ_y) (with respect to the upwind and downwind directions) defined as $\langle e^{jQ_z(x\gamma_x+y\gamma_y)}\rangle$ ($Q_z\in\mathbb{R}$). Then, for statistics up to third order [no peakedness and $(c_{04},c_{40},c_{22}) = (0,0,0)$], from [3], we have

$$\begin{aligned}&\langle e^{jQ_z(x\gamma_x+y\gamma_y)}\rangle\\ &= \int p_{s2}(\gamma_x,\gamma_y)e^{jQ_z(x\gamma_x+y\gamma_y)}d\gamma_x d\gamma_y\\ &= e^{-\frac{Q_z^2}{2}\left(\sigma_{sx}^2x^2+\sigma_{sy}^2y^2\right)}\left[1+\frac{jQ_z^3}{6}x\sigma_{sx}\left(x^2\sigma_{sx}^2c_{03}+3y^2\sigma_{sy}^2c_{21}\right)\right].\end{aligned} \tag{13}$$

For $\boldsymbol{r}\to\boldsymbol{0}$, we have $z_2 - z_1 \approx \gamma_x x + \gamma_y y$ and $\sigma_z^2 - C_z(\boldsymbol{r}) \approx (x^2\sigma_{sx}^2 + y^2\sigma_{sy}^2)/2$ [since $C_z(\boldsymbol{r})$ is an even function, for $\boldsymbol{r}=\boldsymbol{0}$, $\partial_{1,0}C_z = 0$, $\partial_{0,1}C_z = 0$, $\partial_{2,0}C_z = -\sigma_{sx}^2$, and $\partial_{0,2}C_z = -\sigma_{sy}^2$, where $\partial_{n,m} = \partial^{n+m}/\partial x^n\partial y^n$] where $(\sigma_{sx}^2,\sigma_{sy}^2)$ are the surface slope variances along the upwind and downwind directions, respectively. In addition, from [3], we have

$$\begin{aligned}&\lim_{\boldsymbol{r}\to\boldsymbol{0}}\langle\exp[jQ_z(z_2-z_1)]\rangle\\ &\quad\approx\langle\exp[jQ_z(\gamma_x x+\gamma_y y)]\rangle\\ &\quad\approx e^{-\frac{Q_z^2}{2}\left(\sigma_{sx}^2x^2+\sigma_{sy}^2y^2\right)}\times\left[1+jQ_z^3C_s(\boldsymbol{r})\right].\end{aligned} \tag{14}$$

The comparison of (14) with (13) leads for $\boldsymbol{r}\to\boldsymbol{0}$ to

$$C_s(\boldsymbol{r}) = \frac{1}{6}x\sigma_{sx}\left(x^2\sigma_{sx}^2c_{03}+3y^2\sigma_{sy}^2c_{21}\right). \tag{15}$$

In polar coordinates ($x = r\cos\phi$, $y = r\sin\phi$), the above equation becomes

$$\begin{aligned}C_s(r,\phi) &= \frac{r^3\sigma_{sx}}{6}\cos(\phi)\sigma_{sx}\left(\sigma_{sx}^2c_{03}\cos^2\phi+3\sigma_{sy}^2c_{21}\sin^2\phi\right)\\ &= \frac{r^3\sigma_{sx}}{24}[(3a+b)\cos\phi+(a-b)\cos(3\phi)]\end{aligned} \tag{16}$$

where $a = \sigma_{sx}^2c_{03}$ and $b = 3\sigma_{sy}^2c_{21}$.

From [8], [30], and [31], $a\approx b$ and the above equation is simplified as

$$C_s(r,\phi) = \frac{r^3}{6}\sigma_{sx}^3c_{03}\cos\phi. \tag{17}$$

To sum up, the behavior along the angle ϕ is obtained from the symmetry properties of the Cox and Munk slope distribution and explained the general expressions expressed from (4), assumed to be valid for any $\boldsymbol{r}\equiv(r,\phi)$.

Since $C_s(\boldsymbol{r})$ is an odd function, we have

$$\partial_{n,m}C_s|_{\boldsymbol{r}=\boldsymbol{0}} = 0 \quad \text{for}\begin{cases}n \text{ and } m \text{ even}\\ n \text{ and } m \text{ odd}\end{cases} \tag{18}$$

where $\partial_{n,m} = \partial^{n+m}/\partial x^n\partial y^n$. In addition, we can note from (17) that

$$\partial_{n,m}C_s|_{\boldsymbol{r}=\boldsymbol{0}} = 0 \quad \text{for } 0\le n+m\le 2 \tag{19}$$

and

$$\begin{cases}\partial_{3,0}C_s|_{\boldsymbol{r}=\boldsymbol{0}} = \sigma_{sx}^3c_{03}\\ \partial_{1,2}C_s|_{\boldsymbol{r}=\boldsymbol{0}} = \sigma_{sx}^3c_{03}/3\\ \partial_{0,3}C_s|_{\boldsymbol{r}=\boldsymbol{0}} = \partial_{2,1}C_s|_{\mathbf{r}=\mathbf{0}} = 0.\end{cases} \tag{20}$$

C. Skewness and Peakedness Functions for Any r and k

To have a full description of C_s, (16) must be both extrapolated for any $\boldsymbol{r}$ and must satisfy the properties given in (18), (19), and (20). Fung and Chen [32] selected the following form of the skewness function $C_s(r,\phi) = \alpha_s(r\cos\phi)^3\exp(-[r/r_0]^p)$, where $p=1$ in [32] and [33], whereas $p=2$ in [34] and [35]. A dependence of $\cos^3\phi$ is chosen. Guissard [36] pointed out that the determination of r_0 is not based on direct measurements of the skewness. It has seemingly been selected in such a way that the backscattering NRCS agrees with measurements. McDaniel [8] assumed that the skewness spectrum $\hat{C}_s(\boldsymbol{k})$ is expressed in polar coordinates from the isotropic part of the sea height spectrum $\hat{C}_{z0}(k,\psi)$ as $\hat{C}_s(k,\psi) = \hat{C}_{z0}(k)\hat{F}_s(k,\psi)/(2\pi)$. The spectrum $\hat{F}_s$ is determined from the properties given in the previous section. With the help of stereo photographic technique [20], the skewness function is modeled as $C_s(r,\phi) = \alpha_s r^3\exp(-[r/r_0]^p)\cos\phi$, where $r_0\in[15;20]$ cm, $\alpha_s = \sigma_{sx}^3c_{30}/3$ [to satisfy equation (20)], and $p=1$, whereas in [3] and [31], $p=2$.

To satisfy the properties given by (18), (19), and (20), $C_s(r,\phi) = C_{s0}(r)\cos\phi$, in which $C_{s0}(r)$ is assumed to be

$$C_{s0}(r) = \alpha_{s,i}r^3\exp\left(-\left[\frac{r}{l_{s,i}}\right]^i\right)\begin{cases}i=1 & \text{Exponential}\\ i=2 & \text{Gaussian.}\end{cases} \tag{21}$$

Then

$$P_{s0,i} = \alpha_{s,i} l_{s,i}^3 \times \begin{cases} 2 \\ 3\sqrt{\pi}/4 \end{cases} \tag{22}$$

$$r_{\max} = l_{s,i} \times \begin{cases} 3 \\ \sqrt{6}/2 \approx 1.225 \end{cases} \tag{23}$$

and

$$C_{s0}(r_{\max}) = \alpha_{s,i} l_{s,i}^3 \times \begin{cases} 27e^{-3} \approx 1.344 \\ 3\sqrt{3}e^{-3/2}/(2\sqrt{2}) \approx 0.410 \end{cases} \tag{24}$$

where $\{\alpha_{s,i}\}$ $(i = \{1, 2\})$ satisfies from (20)

$$\alpha_{s,i} \approx \frac{\sigma_{sx}^3 c_{30}}{6}. \tag{25}$$

In addition, $r_{\max}$ is the distance, for which the function is maximum.

In the spectral domain, the associated spectrum is expressed from (9) and (10) as $\hat{C}_s(k, \psi) = -j\cos(\psi)\hat{C}_{s0}(k)/(2\pi)$, in which $\hat{C}_{s0}(k)$ is given, from (21), by

$$\hat{C}_{s0}(k) = \alpha_{s,i} l_{s,i}^4 \times \begin{cases} \dfrac{15u^2\left(4 - 3u^2\right)}{\left(1 + u^2\right)^{9/2}} & i = 1 \\ \dfrac{u^2}{16} e^{-\frac{u^2}{4}} \left(u^2 - 8\right) & i = 2 \end{cases} \tag{26}$$

where $u = k l_{s,i}$.

From the Cox and Munk slope distribution, the coefficient $\alpha_{s,i}$ can be determined, whereas the length $l_{s,i}$ remains to determine. From the definition of $l_{s,i}$, it might be considered as the equivalent of the surface height correlation distance, for the surface height correlation function. We shall call it the skewness distance.

IV. Closed-Form Expressions of the NRCS

The determination of the skewness distance l_s is required to calculate C_{s0}. With the help of stereo photographic technique, Mironov *et al.* [20] found $l_s \in [15; 20]$ cm. Using both the data of the Cox and Munk slope distribution for clean and oil slick (the capillary waves are strongly damped) sea surfaces, Elfouhaily [31] found $l_s \approx 1$ cm, whereas Bourlier [3] found $l_s \approx 10$ cm. From measurements of the backscattering NRCS, the Fung's group conducted studies (summarized by Guissard [36]) to determine l_s. It is found that $l_s \in [1; 2]$ cm and l_s depend on the wind speed. This brief review reveals that the values of l_s are spread and they are of the order of the centimeter, which is related to the choice of $C_{s0}(r)$ given by (21).

To obtain a closed-form expression of σ_1, we assume that $\Omega_1(\alpha_1, \alpha_2) \approx -J_1(\alpha_1)$ $(\alpha_2 \approx 0) \approx -\alpha_1/2$ since $|\alpha_1| \ll 1$ from (24) and (25) ($l_{s,i}$ ranges from 0.01 to 0.001 m and $\alpha_{s,i}$ is of the order of 10^{-4}). In addition, since $r_{\max}$ (distance for which the skewness function C_{s0} is maximum) is close to zero and since above this distance, C_{s0} decreases rapidly, $-(Q_z^2\sigma_z^2 - \alpha_0)$ can be expanded as $-Q_z^2[\sigma_z^2 - C_{z0}(0) - C_{z0}''(0)r^2/2] = -Q_z^2\sigma_{s0}^2 r^2/2$, where $\sigma_{s0}^2 = -C_{z0}''(0) = (\sigma_{sx}^2 + \sigma_{sy}^2)/2$ and $C_{z0}'(0) = 0$, since C_{z0} is an even function. With these two approximations, (1) becomes

$$\begin{aligned} \sigma_1 &\approx -2Q_z|\mathcal{B}_1|^2 \int_0^\infty e^{-Q_z^2\left[\sigma_z^2 - C_{z0}(r)\right]} C_{s0}(r) J_1(Q_H r) r dr \\ &\approx -2Q_z|\mathcal{B}_1|^2 \int_0^\infty e^{-\frac{Q_z^2\sigma_{s0}^2 r^2}{2}} C_{s0}(r) J_1(Q_H r) r dr. \end{aligned} \tag{27}$$

From Appendix C, the above equation can also expressed in the spectral domain.

For a Gaussian-like Skewness function, introducing the equivalent distance $L_{\text{eq},2}$ as $1/L_{\text{eq},2}^2 = 1/l_{s,2}^2 + 1/L_g^2$, where $L_g = \sqrt{2}/(Q_z\sigma_{s0})$, from (10), the substitution of (21) into (27) leads to

$$\sigma_1 = -2Q_z|\mathcal{B}_1|^2 \frac{\hat{C}_{s0}(u)}{Q_H} \tag{28}$$

where $\hat{C}_{s0}$ is expressed from (26) $(i = 2)$, $u = Q_H L_{\text{eq},2} = Q_{H,s} l_{s,2}$, where $Q_{H,s} = Q_H L_g/(L_g^2 + l_{s,2}^2)^{1/2}$. Like the first-order SPM for the coefficients $\{\sigma_{0,2}\}$, σ_1 is proportional to the skewness spectrum, but at a modified Bragg wavenumber $Q_{H,s}$, which depends on the intrinsic parameters of the sea surface $\{\sigma_{s0}, L_{s,2}\}$, unlike Q_H. If $L_g \to \infty$, then $Q_{H,s} \to Q_H$.

For an exponential profile of the skewness function, the integration over r cannot make analytically. But, as the integrand contributes for small values of r because $l_{s,1} \ll L_g$, in (27), the exponential term can be expanded as $e^{-r^2/L_g^2} \approx 1 - r^2/L_g^2 + r^4/(2L_g^4)$. From (27), this leads to

$$\sigma_1 \approx -2Q_z|\mathcal{B}_1|^2 \int_0^\infty \left(1 - \frac{r^2}{L_g^2} + \frac{r^4}{2L_g^4}\right) C_{s0}(r) J_1(Q_H r) r dr. \tag{29}$$

The integration over r is reported in Appendix B. For any spatial skewness function, the substitution of (B1) into (29) leads to

$$\sigma_1 \approx -2Q_z|\mathcal{B}_1|^2 \left(\frac{\hat{C}_{s0}(Q_H)}{Q_H} - \frac{F_1(Q_H)}{L_g^2} + \frac{F_2(Q_H)}{2L_g^4}\right) \tag{30}$$

where F_1 and F_2 are defined from (B2) and (B3), which depend on the derivatives of the skewness spectrum $\hat{C}_{s0}$.

For an exponential profile defined by (21), the functions F_1 and F_2 are

$$\begin{cases} F_1 = \dfrac{315 l_{s,1}^7 u(8 - 20u^2 + 5u^4)}{(u^2 + 1)^{13/2}} \\ F_2 = \dfrac{2835 l_{s,1}^9 u(64 - 336u^2 + 280u^4 - 35u^6)}{(u^2 + 1)^{17/2}} \end{cases} \tag{31}$$

where $u = k l_{s,1}$.

V. Numerical Results

In this section, first, the closed-form expressions of σ_1 expressed from (27) (first line), (28) (Gaussian case), and (30) (exponential case) are compared with (1), in which the integration over r is done numerically without approximation in the integrand. Second, the results computed from (1) are compared with experimental data in C [27], [28] and K_u [26], [29] bands.

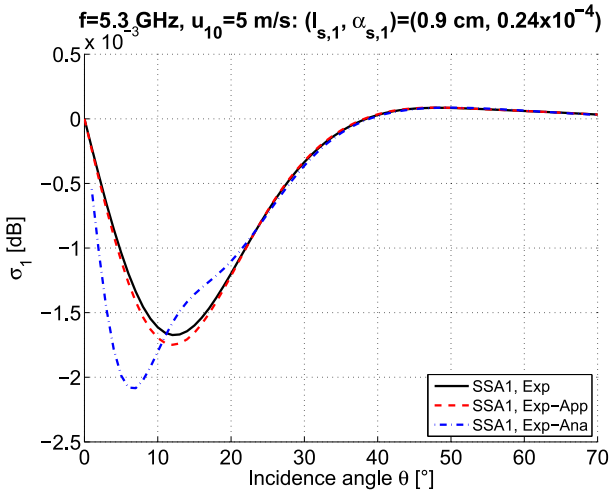

(a)

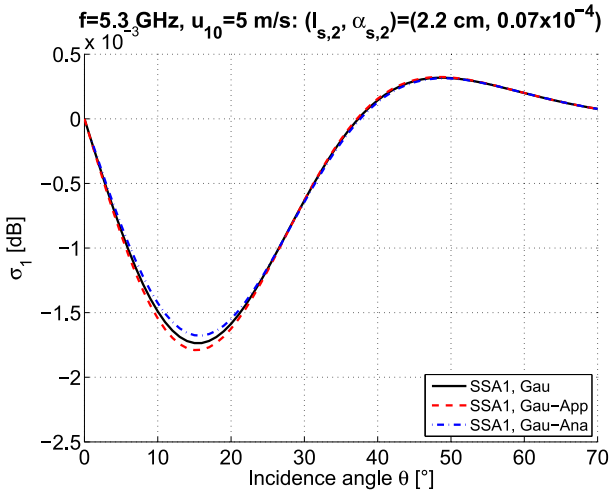

(b)

Fig. 1. Coefficient σ_1 versus the incidence angle θ in dB scale. The polarization is VV, $f = 5.3$ GHz and $u_{10} = 5$ m/s. (a) Exponential. (b) Gaussian.

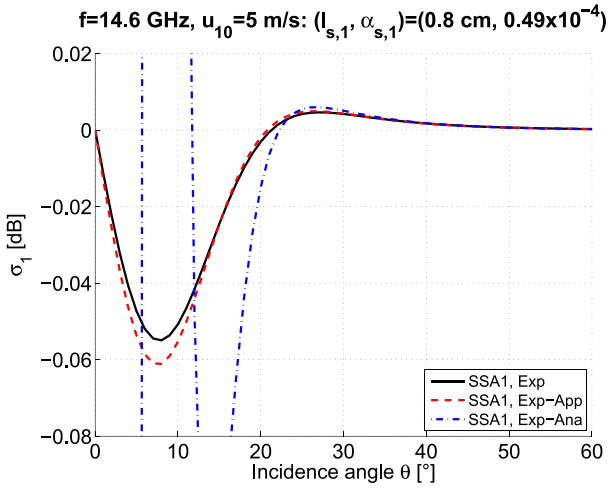

(a)

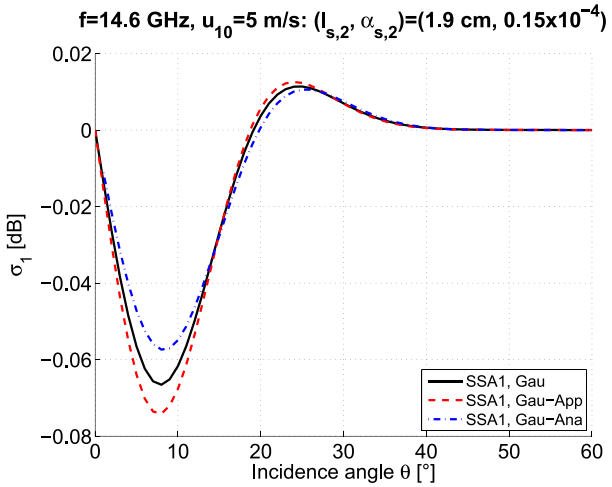

(b)

Fig. 2. Similar variations as in Fig. 1 but the frequency is $f = 14.6$ GHz. (a) Exponential. (b) Gaussian.

A. Comparison of the NRCSs

Fig. 1 plots the coefficient σ_1 versus the incidence angle θ in dB scale for $f = 5.3$ GHz and $u_{10} = 5$ m/s. The legend in the figure is as follows.

1) The label "SSA1, Exp" means that σ_1 is computed from (1), in which the spatial skewness function $C_{s0}(r)$ has an exponential profile.
2) The label "SSA1, Exp-App" means that σ_1 is computed from (27) (first line), in which the spatial skewness function $C_{s0}(r)$ has an exponential profile.
3) The label "SSA1, Exp-Ana" means that σ_1 is computed from (30) (exponential profile).
4) The label "SSA1, Gau" means that σ_1 is computed from (1), in which the spatial skewness function $C_{s0}(r)$ has a Gaussian profile.
5) The label "SSA1, Gau-App" means that σ_1 is computed from (27) (first line), in which the spatial skewness function $C_{s0}(r)$ has a Gaussian profile.
6) The label "SSA1, Gau-Ana" means that σ_1 is computed from (28) (Gaussian profile).

Fig. 2 plots the same variations as in Fig. 1, but the frequency is $f = 14.6$ GHz.

To reduce the surface curvature effect, not well accounted for in the SSA1 model, the VV polarization is chosen as this effect is stronger for the HH polarization. To have the same power $P_{s0,i}$ given by (11), the coefficient $\alpha_{s,1}$ of the exponential profile is multiplied by $\alpha_{s,2}P_{s,2}/P_{s,1} = \sqrt{\pi}\alpha_{s,2}(l_{s,2}/l_{s,1})^3/8$. In the same way, we choose that the abscissa of the spatial skewness functions, for which they are maxima, is equal. Then, from (23), $l_{s,1} = l_{s,2}/\sqrt{6} \approx 0.408 l_{s,2}$. The numerical values (obtained in the subsection by fitting σ_1 with experimental data) are listed in the title of each figure.

Figs. 1 and 2 show that for incidence angles near the nadir σ_1 is negative to reach the minimum and next increases to reach the maximum, which is positive and of level smaller than the absolute value of the minimum, and converges asymptotically to zero as the incidence angle increases. The level of the maximum is larger for the Gaussian profile and then σ_1 converges to zero more slowly than that of the exponential profile.

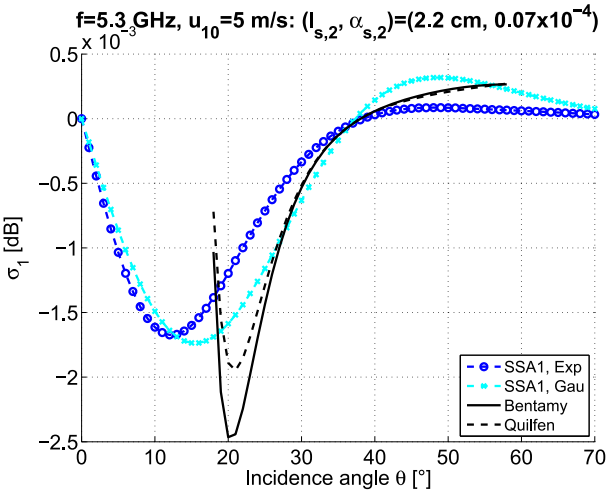

(a)

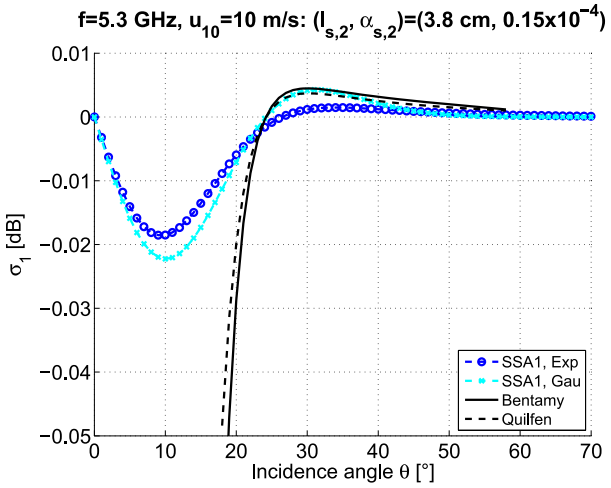

(b)

Fig. 3. Coefficient σ_1 versus the incidence angle θ in dB scale. The polarization is VV, $f = 5.3$ GHz and $u_{10} = \{5, 10\}$ m/s. (a) $u_{10} = 5$ m/s. (b) $u_{10} = 10$ m/s.

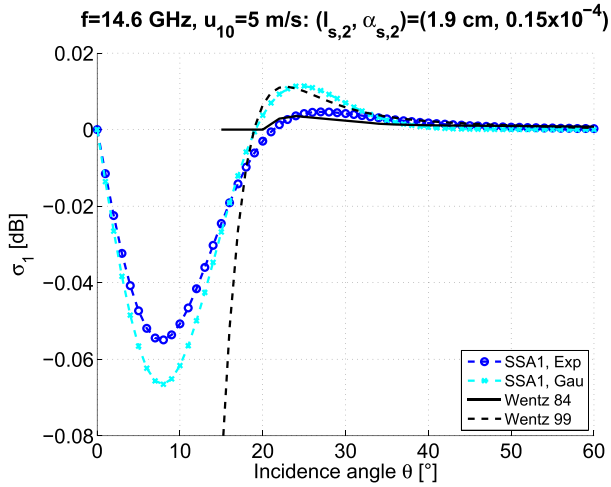

(a)

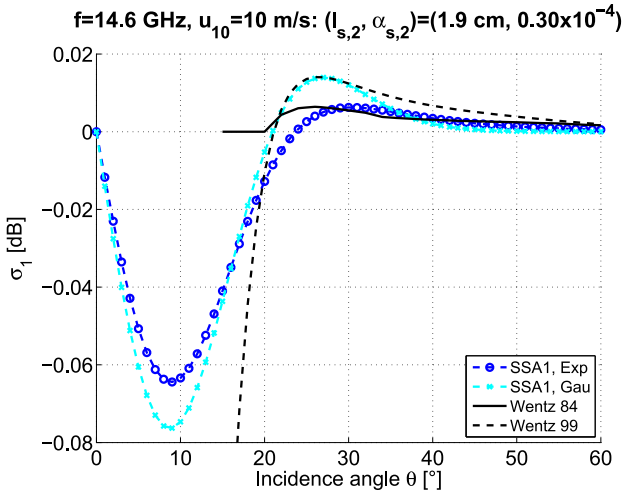

(b)

Fig. 4. Similar variations as in Fig. 3 but the frequency is $f = 14.6$ GHz. (a) Exponential. (b) Gaussian.

Figs. 1 and 2 also show that the "SSA1, Exp-App" or "SSA1, Gau-App" results $(-J_1(\alpha_1) \approx -\alpha_1/2 = -jQ_z^3 C_{s0}(r)/2)$ match well with those of σ_1, for which no assumption is used. However, as the surface roughness $Q_z = 2K\sigma_z \cos\theta$ (Rayleigh parameter) increases (frequency f or/and wind speed u_{10}), the "SSA1, Exp-Ana" or "SSA1, Gau-Ana" results deviate from those of "SSA1" without approximation and the difference is larger for the exponential profile since a Taylor series expansion is applied on $e^{-Q_z^2[\sigma_z^2 - C_{z0}(r)]}$, unlike the Gaussian case.

B. Comparison With Data

First simulations, not depicted here, showed that the values of $\alpha_{s,2}$ computed from the Cox and Munk model [1] [$c_{03} = (3.3\ u_{12} - 4 \pm 6) \times 10^{-2}$ where $u_{12} \approx u_{10}$] overestimates σ_1 in comparison to the measurements. An inversion simple scheme is then proposed to perform $\alpha_{s,2}$ and $l_{s,2}$ from the experimental data. First, $l_{s,2}$ is determined from the value of Q_{H_0}, for which σ_1 equals zero. This implies, from (28), that $L_{2,\mathrm{eq}} Q_{H_0} = u_0 = 2\sqrt{2} \Rightarrow L_{2,\mathrm{eq}} = 2\sqrt{2}/Q_{H_0}$ and

$$l_{s,2} = \left(\frac{1}{L_{2,\mathrm{eq}}^2} - \frac{Q_{z_0}^2 \sigma_{s0}^2}{2} \right)^{-1/2} \tag{32}$$

where $Q_{z_0} = (1 - Q_{H_0}^2)^{1/2}$.

The data showed a maximum of σ_1, which occur from (28) $[\sigma_1'(u_1) = 0]$ at $u_1 \approx 3.570$, and the corresponding value of $u(u^2 - 8)e^{-u^2/4}$ is approximately 0.700. Then, from (26) $(i = 2)$ and (29), we have

$$\alpha_{s,2} \approx \left. \frac{8}{0.7 Q_z |\mathcal{B}_1|^2 L_{eq,2}^5} \right|_{u=u_1}. \tag{33}$$

Figs. 1 and 4 plot the coefficient σ_1 versus the incidence angle θ in dB scale for $f = \{5.3, 14.6\}$ GHz and $u_{10} = \{5, 10\}$ m/s. The legend in the figure is as follows.

1) The label "Bentamy" means that σ_1 is computed from the data provided in [28] ($f = 5.3$ GHz and $\theta \in [18; 58]°$).

2) The label "Quilfen" means that σ_1 is computed from the data provided in [27] ($f = 5.3$ GHz and $\theta \in [18; 58]°$).
3) The label "Wentz 84" means that σ_1 is computed from the data provided in [26] ($f = 14.6$ GHz and $\theta \in [0; 60]°$). The negative values are forced to set zeros by the authors.
4) The label "Wentz 99" means that σ_1 is computed from the data provided in [26] ($f = 14.6$ GHz and $\theta \in [15; 60]°$).

In the region of negative values, Figs. 3 and 4 show that the data decrease more rapidly than the simulated results. In addition, in Fig. 3(a), a local minimum occurs for the data, which is shifted toward the higher values and of lower level in comparison to the simulated results.

Near the nadir, it is important to underline that the coefficient σ_0 is much larger than σ_1, and then, σ_1 can be comparable to the noise level. The measurement of σ_1 near the nadir requires a very good precision of the measured levels.

For the two frequencies, $\alpha_{s,2}$ is approximatively multiplied by 2 from $u_{10} = 5$ m/s to $u_{10} = 10$ m/s, like $l_{s,2}$ for only $f = 5.3$ GHz, whereas for $f = 14.6$ GHz, $l_{s,2}$ is constant. In comparison to the Cox and Munk measurements [1], $\alpha_{s,2} \in [1.4; 4.1]\times 10^{-4}$ and $\alpha_{s,2} \in [5.0; 7.7]\times 10^{-4}$ for $u_{10} = \{5, 10\}$ m/s, respectively, which is 10–20 times larger than the values obtained from fitting the data.

VI. Conclusion

In this paper, from the first-order SSA, the first-order coefficient of the Backscattering NRCS along the harmonic $\cos\phi$ is derived by introducing the azimuthal property of the skewness function. In addition, by introducing the assumption that the skewness correlation distance is much smaller than that of the gravity waves, the integration over the radial distance is performed analytically. The proposed approaches are compared with experimental data in C and K_u bands. For moderate incidence angles, the comparisons showed a satisfactory agreement.

As the levels of σ_1 are small, it requires a very good precision of the measurements, mostly near the nadir, for which the backscattering NRCS coefficient σ_0 is much larger.

Appendix A
Integration Over the Azimuthal Direction

From [37], we have

$$e^{jacos(\phi-\psi)} = \sum_{n=-\infty}^{n=+\infty} j^n J_n(a) e^{jn(\phi-\psi)} \tag{A1}$$

where J_n is the Bessel function of nth order and of the first kind. Then

$$\begin{aligned}\int_0^{2\pi} & e^{jp\psi} e^{ja\cos(\phi-\psi)} d\psi \\ &= \sum_{n=-\infty}^{n=+\infty} j^n J_n(a) e^{jn\phi} \times \int_0^{2\pi} e^{j(p-n)\psi} d\psi \\ &= 2\pi \sum_{n=-\infty}^{n=+\infty} j^n J_n(a) e^{jn\phi} \delta_{n,p} \\ &= 2\pi j^p J_p(a) e^{jp\phi}\end{aligned} \tag{A2}$$

where $\delta_{n,p}$ is the Kronecker symbol defined as $\delta_{n,p} = 1$ if $n = p$, 0 otherwise. In addition, since $\cos\alpha = (e^{j\alpha} + e^{-j\alpha})/2$, we have

$$\int_0^{2\pi} \cos(p\phi) e^{ja\cos(\phi-\psi)} d\psi = 2\pi j^p \cos(p\phi) J_p(a) \tag{A3}$$

since $J_{-p}(a) = (-1)^p J_p(a)$ and $j^{-p} = j^p(-1)^p$.

Appendix B
Integration Over the Radial Distance

In (29), to perform the integration over r, the following two integrals are introduced:

$$\begin{cases} G_n = \displaystyle\int_0^{\infty} r^{2n} C_{s0}(r) J_0(kr) dr \\ F_n = \displaystyle\int_0^{\infty} r r^{2n} C_{s0}(r) J_1(kr) dr = -\frac{dG_n}{dk} \end{cases} \tag{B1}$$

and from (10), $F_0 = \hat{C}_{s0}(k)/k$. In addition, from (10), we have

$$\begin{aligned}\frac{d\hat{C}_{s0}}{dk} &= \hat{C}'_{s0} = k\int_0^{\infty} r^2 C_{s0}(r) J_0(kr) dr = kG_1 \\ &\Rightarrow G_1 = \frac{\hat{C}'_{s0}}{k} \Rightarrow F_1 = -\frac{d}{dk}\left(\frac{\hat{C}'_{s0}}{k}\right) \\ &\Rightarrow F_1 = \frac{\hat{C}'_{s0} - k\hat{C}''_{s0}}{k^2}\end{aligned} \tag{B2}$$

and

$$\begin{aligned}\frac{d^3\hat{C}_{s0}}{dk^3} &= \hat{C}'''_{s0} = -\int_0^{\infty} [r^3 J_1(kr) + kr^4 J_0(kr)] C_{s0}(r) dr \\ &= -F_1 - kG_2 \\ &\Rightarrow G_2 = -\frac{\hat{C}'''_{s0} + F_1}{k} \Rightarrow F_2 = \frac{d}{dk}\left(\frac{\hat{C}'''_{s0} + F_1}{k}\right) \\ &\Rightarrow F_2 = \frac{k^3\hat{C}''''_{s0} - 2k^2\hat{C}'''_{s0} + 3k\hat{C}''_{s0} - 3\hat{C}'_{s0}}{k^4}.\end{aligned} \tag{B3}$$

Appendix C
Backscattering NRCS in the Spectral Domain

From (27) (second line) and (12), σ_1 is expressed as

$$\sigma_1 = -2Q_z|\mathcal{B}_1|^2 \int_0^{\infty}\int_0^{\infty} e^{-\frac{r^2}{L_g^2}} \hat{C}_{s0}(k) J_1(Q_H r) J_1(kr) r dr dk \tag{C1}$$

where $1/L_g^2 = Q_z^2\sigma_{s0}^2/2$. From [37], the derivation of the integration over r leads to

$$\sigma_1 = -Q_z|\mathcal{B}_1|^2 L_g^2 \int_0^{\infty} e^{-\frac{L_g^2(k^2+Q_H^2)}{4}} I_1\left(\frac{L_g^2 Q_H k}{2}\right) \hat{C}_{s0}(k) dk. \tag{C2}$$

It is interesting to study the case for which $L_g \to \infty$. As $I_1(z) \approx e^z/\sqrt{2\pi z}$ for $z \to \infty$, the above equation is simplified as

$$\sigma_1 = -\frac{Q_z|\mathcal{B}_1|^2 L_g}{\sqrt{\pi}} \int_0^{\infty} \frac{1}{\sqrt{Q_H k}} e^{-\frac{L_g^2(k-Q_H)^2}{4}} \hat{C}_{s0}(k) dk. \tag{C3}$$

The use of the variable transformation $u = L_g(k - Q_H)/2$ leads to

$$\sigma_1 = -2Q_z|\mathcal{B}_1|^2 \frac{1}{\sqrt{Q_H \pi}} \int_{-L_g Q_H/2}^{\infty} e^{-u^2} \frac{\hat{C}_{s0}(k)}{\sqrt{k}} du \qquad \text{(C4)}$$

where $k = Q_H + 2u/L_g$. Since $L_g \to \infty$, $k \approx Q_H$ and $-L_g Q_H/2 \to -\infty$. Then, the term $\hat{C}_{s0}(k)/\sqrt{k} \approx \hat{C}_{s0}(Q_H)/\sqrt{Q_H}$ can come out of the integral and the integration over u gives $\sqrt{\pi}$. In conclusion, as $L_g \to \infty$, σ_1 is simplified as

$$\sigma_1 = -2Q_z|\mathcal{B}_1|^2 \frac{\hat{C}_{s0}(Q_H)}{Q_H}. \qquad \text{(C5)}$$

This approximation corresponds to the first-order SPM.

REFERENCES

[1] C. Cox and W. Munk, "Statistics of the sea surface derived from sun glitter," *J. Marine Res.*, vol. 13, no. 2, pp. 198–227, 1954.

[2] A. G. Voronovich, V. U. Zavorotny, and V. G. Irisov, "Sea-roughness spectrum retrieval from radar and radiometric measurements," in *Proc. Int. Geosci. Remote Sens. Symp.*, Piscataway, NJ, USA, Jul. 2000, pp. 3102–3104.

[3] C. Bourlier, "Azimuthal harmonic coefficients of the microwave backscattering from a non-Gaussian ocean surface with the first-order SSA model," *IEEE Trans. Geosci. Remote Sens.*, vol. 42, no. 11, pp. 2600–2611, Nov. 2004.

[4] C. Bourlier, N. Déchamps, and G. Berginc, "Comparison of asymptotic backscattering models (SSA, WCA, and LCA) from one-dimensional Gaussian ocean-like surfaces," *IEEE Trans. Antennas Propag.*, vol. 53, no. 5, pp. 1640–1652, May 2005.

[5] A. G. Voronovich, "Small-slope approximation for electromagnetic wave scattering at a rough interface of two dielectric half-spaces," *Waves Random Media*, vol. 4, no. 3, pp. 337–367, 1994.

[6] A. G. Voronovich and V. U. Zavorotny, "Theoretical model for scattering of radar signals in K_u- and C-bands from a rough sea surface with breaking waves," *Waves Random Media*, vol. 11, no. 3, pp. 247–269, 2001.

[7] S. T. McDaniel, "Small-slope predictions of microwave backscatter from the sea surface," *Waves Random Media*, vol. 11, no. 3, pp. 343–360, 2001.

[8] S. T. McDaniel, "Microwave backscatter from non-Gaussian seas," *IEEE Trans. Geosci. Remote Sens.*, vol. 41, no. 1, pp. 52–58, Jan. 2003.

[9] C. Bourlier and N. Pinel, "Numerical implementation of local unified models for backscattering from random rough sea surfaces," *Waves Random Complex Media*, vol. 19, no. 3, pp. 455–479, Aug. 2009.

[10] C. Bourlier and N. Pinel, "Low-frequency limit of unified models for backscattering from oceanlike surfaces," *IEEE Geosci. Remote Sens. Lett.*, vol. 7, no. 3, pp. 506–510, Jul. 2010.

[11] A. G. Voronovich and V. U. Zavorotny, "Full-polarization modeling of monostatic and bistatic radar scattering from a rough sea surface," *IEEE Trans. Antennas Propag.*, vol. 62, no. 3, pp. 1362–1371, Mar. 2014.

[12] T. Elfouhaily, S. Guignard, R. Awadallah, and D. R. Thompson, "Local and non-local curvature approximation: A new asymptotic theory for wave scattering," *Waves Random Media*, vol. 13, no. 4, pp. 321–337, 2003.

[13] T. Elfouhaily, C. Bourlier, and J. T. Johnson, "Two families of non-local scattering models and the weighted curvature approximation," *Waves Random Media*, vol. 14, no. 4, pp. 563–580, 2004.

[14] C.-A. Guérin, G. Soriano, and T. Elfouhaily, "Weighted curvature approximation: Numerical tests for 2D dielectric surfaces," *Waves Random Media*, vol. 14, no. 3, pp. 349–363, Jul. 2004.

[15] C.-A. Guérin, G. Soriano, and B. Chapron, "The weighted curvature approximation in scattering from sea surfaces," *Waves Random Complex Media*, vol. 20, no. 3, pp. 364–384, 2010.

[16] A. A. Mouche, B. Chapron, and N. Reul, "A simplified asymptotic theory for ocean surface electromagnetic wave scattering," *Waves Random Complex Media*, vol. 17, no. 3, pp. 321–341, 2007.

[17] A. A. Mouche, B. Chapron, N. Reul, D. Hauser, and Y. Quilfen, "Importance of the sea surface curvature to interpret the normalized radar cross section," *J. Geophys. Res., Oceans*, vol. 112, no. C10, pp. C10002-1–C10002-12, 2007.

[18] B. F. Kur'yanov, "The scattering of sound at a rough surface with two types of irregularity," *Sov. Phys. Acoust.*, vol. 8, no. 3, pp. 252–257, 1963.

[19] J. Wright, "A new model for sea clutter," *IEEE Trans. Antennas Propag.*, vol. 16, no. 2, pp. 217–223, Mar. 1968.

[20] A. S. Mironov, M. V. Yurovskaya, V. A. Dulov, D. Hauser, and C. A. Guérin, "Statistical characterization of short wind waves from stereo images of the sea surface," *J. Geophys. Res., Oceans*, vol. 117, no. C12, pp. C00J35-1–C00J35-16, 2012.

[21] G. Caulliez and C.-A. Guérin, "Higher-order statistical analysis of short wind wave fields," *J. Geophys. Res., Oceans*, vol. 117, no. C6, pp. C06002-1–C06002-14, 2012.

[22] J. A. Shaw and J. H. Churnside, "Scanning-laser glint measurements of sea-surface slope statistics," *Appl. Opt.*, vol. 36, no. 18, pp. 4202–4213, 1997.

[23] R. Lawner and R. Moore, "Short gravity and capillary wave spectra from tower-based radar," *IEEE J. Ocean. Eng.*, vol. OE-9, no. 5, pp. 317–324, Dec. 1984.

[24] A. Bringer, C.-A. Guérin, B. Chapron, and A. A. Mouche, "Peakedness effects in near-nadir radar observations of the sea surface," *IEEE Trans. Geosci. Remote Sens.*, vol. 50, no. 9, pp. 3293–3301, Sep. 2012.

[25] A. Bringer, B. Chapron, A. Mouche, and C.-A. Guérin, "Revisiting the short-wave spectrum of the sea surface in the light of the weighted curvature approximation," *IEEE Trans. Geosci. Remote Sens.*, vol. 52, no. 1, pp. 679–689, Jan. 2014.

[26] F. J. Wentz, S. Peteherych, and L. A. Thomas, "A model function for ocean radar cross sections at 14.6 GHz," *J. Geophys. Res., Oceans*, vol. 89, no. C3, pp. 3689–3704, 1984.

[27] Y. Quilfen, B. Chapron, T. Elfouhaily, K. Katsaros, and J. Tournadre, "Observation of tropical cyclones by high-resolution scatterometry," *J. Geophys. Res., Oceans*, vol. 103, no. C4, pp. 7767–7786, 1998.

[28] A. Bentamy, P. Queffeulou, Y. Quilfen, and K. Katsaros, "Ocean surface wind fields estimated from satellite active and passive microwave instruments," *IEEE Trans. Geosci. Remote Sens.*, vol. 37, no. 5, pp. 2469–2486, Sep. 1999.

[29] F. J. Wentz and D. K. Smith, "A model function for the ocean-normalized radar cross section at 14 GHz derived from NSCAT observations," *J. Geophys. Res., Oceans*, vol. 104, no. C5, pp. 11499–11514, 1999.

[30] M. S. Longuet-Higgins, "On the skewness of sea-surface slopes," *J. Phys. Oceanogr.*, vol. 12, no. 11, pp. 1283–1291, 1982.

[31] T. Elfouhaily, "A consistent wind and wave model and its application to microwave remote sensing of the ocean surface," Ph.D. dissertation, Dept. Phys., Paris Diderot Univ., Paris, France, 1997.

[32] A. K. Fung and K. S. Chen, "Kirchhoff model for a skewed random surface," *J. Electromagn. Waves Appl.*, vol. 5, no. 2, pp. 205–216, 1991.

[33] K. S. Chen, A. K. Fung, and D. E. Weissman, "A backscattering model for ocean surface," *IEEE Trans. Geosci. Remote Sens.*, vol. 30, no. 4, pp. 811–817, Jul. 1992.

[34] A. K. Fung, *Microwave Scattering and Emission Models and Applications* (Remote Sensing Library). Boston, MA, USA: Artech House, 1994.

[35] K. S. Chen, A. K. Fung, and F. Amar, "An empirical bispectrum model for sea surface scattering," *IEEE Trans. Geosci. Remote Sens.*, vol. 31, no. 4, pp. 830–835, Jul. 1993.

[36] A. Guissard, "Multispectra for ocean-like random rough surface scattering," *J. Electromagn. Waves Appl.*, vol. 10, no. 10, pp. 1413–1443, 1996.

[37] M. Abramowitz and I. A. Stegun, Eds., *Handbook of Mathematical Functions*. New York, NY, USA: Dover, 1970.

Christophe Bourlier was born in La Flèche, France, in 1971. He received the M.S. degree in electronics from the University of Rennes 1, Rennes, France, in 1995, and the Ph.D. degree from the Système Électronique et Informatique Laboratory, Nantes, France.

He is currently with the Institute of Electronics and Telecommunications of Rennes Laboratory, Polytech Nantes, University of Nantes, Nantes, France. He is a Researcher with the National Center for Scientific Research, Nantes, France, where he is involved in electromagnetic wave scattering from rough surfaces (ocean-like surfaces) and objects for microwaves and infrared remote sensing applications and radar signatures. He has authored more than 200 journal articles and conference papers.